Quantitative assessment of flooding risk based on predicted evacuation time: A case study in Joso city, Japan

Han, Zishuang
Department of Civil Engineering, Graduate School of Engineering, Kyushu University

Mitani, Yasuhiro
Disaster Risk Reduction Research Center, Graduate School of Engineering, Kyushu University

Kawano, Kohei
Disaster Risk Reduction Research Center, Graduate School of Engineering, Kyushu University

Taniguchi, Hisatoshi
Disaster Risk Reduction Research Center, Graduate School of Engineering, Kyushu University

他

https://hdl.handle.net/2324/7173153

出版情報：International Journal of Disaster Risk Reduction. 98, pp.104113-, 2023-11. Elsevier
バージョン：
権利関係：

Abstract

Flooding is a frequent natural hazard, threatening people's lives and properties worldwide. Even though completely preventing damage from flooding is impossible, an appropriate evacuation can help minimize its impact and mitigate human casualties. However, analyzing various flooding information to make quick evacuation judgments is challenging for decision-makers. Therefore, a quantitative flooding risk assessment is needed to support appropriate evacuation decisions. This study introduces the travel time under ideal evacuation conditions to quantify evacuation vulnerability, with Dijkstra's algorithm finding the evacuation route and the Random Forest algorithm predicting the evacuation time. The evacuation vulnerability is then integrated with time-varying flooding hazards and estimated congestion levels to assess evacuation risk. Herein, a case study in Joso, Japan is used as an example to demonstrate the practicality and applicability of the proposed approach. As a result, the prediction model achieved high accuracy with an RMSE of 0.88min and a MAPE of 5.88%. The proposed approach clearly illustrated the vulnerable areas and times that may hinder an efficient evacuation process. Also, this approach identified and visualized the individual evacuation risk distribution during the flooding scenario: 49.38% of buildings were assessed as having no evacuation ability, while a maximum of 11.86% and 3.83% of the buildings were assessed as middle-risk and high-risk. Furthermore, the regional evacuation deadline and priorities were specified to ensure timely and effective evacuation. Overall, this study develops an approach for assessing evacuation vulnerability and risk that could facilitate awareness among the public and provide judgmental bases for evacuation preparedness and decision-making.

Keywords: Flood risk, Quantitative assessment, Evacuation time prediction, Dijkstra's algorithm, Random Forest algorithm

1. Introduction

Flooding, one of the most widespread natural hazards, threatens people's lives and properties worldwide [1,2]. According to a 2015 report by the UN Office for Disaster Risk Reduction [3], floods accounted for 47% of all weather-related disasters during 1995-2015. These disasters were responsible for approximately 157,000 casualties. Unfortunately, several studies have indicated that flooding is becoming more frequent and intense due to global warming, climate change, and sea-level rise [4–7]. Furthermore, rapid urbanization in the 21st century has increased the density of both population and property while significantly increasing the exposure to flooding [8,9].

Even though the flooding disaster cannot be prevented entirely, an appropriate evacuation can help minimize the disaster's impact and mitigate human casualties [10,11]. Evacuation, one of the most critical preparedness measures for public protection, is usually the first choice in the emergency response [12–15]. However, when a disaster occurs, analyzing complex information to make quick judgments is a challenging task for decision-makers [16,17]. In past disaster evacuations, there were cases where some residents failed to evacuate at the appropriate time because of improper evacuation notifications. There were also cases where residents in dangerous areas did not evacuate due to distrust or neglect of the issued notifications [18–20]. Investigations have indicated that these unappropriated evacuations may threaten evacuees' safety and cause fatalities during emergencies [10,21–23]. Therefore, providing a quantitative risk assessment to support appropriate and trustworthy evacuation decisions is essential [24–28].

Conventionally, the disaster risk was considered as a measure of losses in terms of socio-economic impacts from a potential calamity, and there are mainly four assessment approaches [29]: the first is historical-record-based analysis, which is based on the statistics of historical flood events but requires sufficient historical records and may be inaccurate in assessing the spatial distribution of flood risk [30–32]; The second is multi-criteria-based analysis, which depends on experts' judgments to make decisions but has limitations in the determination of subjective factors [33–35]; The third is Geographical Information System(GIS) & Remote Sensing(RS)-based analysis, which can map the spatial distribution of comprehensive flood risk but demands high resolution input data. [24,36–38]; The last is scenario-based analysis, which can be used in different scenarios with changing spatial domains and combine various data to predict flood risk immediately before an occurrence [39–41]. These four approaches provide great theoretical support for risk assessment. Among them, GIS&RS-based and scenario-based analyses have been widely used in regional flood risk assessing and mapping [38]. These risk assessments effectively provided information about safe and unsafe areas, potential losses, and exposures to natural hazards. However, drawing direct conclusions from these traditional social-economic focused research is difficult due to their different purposes [42–46].

Since evacuation mainly serves to appropriately shift evacuees from dangerous areas to safer areas or shelters, sound decisions on when and where to evacuate are critical [29,47,48]. In the last 40 years, evacuation-related risk has been proposed as a new perspective of risk assessment, such as using the potential inability to evacuate to define risk [12,29,43,44,49,50]. One commonly used model is the Critical Cluster Model (CCM), proposed by Cova and Church. The CCM assessed pre-disaster evacuation risk by considering potential obstacles to the evacuation process [43,44,51]. Chen developed a new assessment approach that extended the CCM to model evacuation risk, which considered not only pre-disaster factors but also the disaster distance and evacuees' routing behaviors during the post-disaster [29]. Zhao proposed a comprehensive risk assessment method based on nuclear radiation concentration and vulnerability of traffic evacuation [16]. Hsu and Peeta calculated the evacuation risk of a location as the time margin available to clear a location before a disaster by the dynamics of evacuation traffic flows [49,52,53].

Considering the transportation system is a central component during evacuation, the quantitative risk assessment focusing on evacuation time in the road network is important to timely evacuation, where identifying the required time to reach evacuation destinations is essential [54]. Existing research on estimating road travel time—both evacuation-related and beyond—can be summarized into four main approaches: the first is the microscopic simulation-based method, which can encompass the evacuees' movements and traffic flow to provide accurate estimates. There are already numerous mature microsimulation software products, such as Netlogo, STEPS, and MATSim. However, realizing the large-scale simulation demands high computational complexity, computing time, and detailed input[51,54,55]; the second is the mathematical-based model, which is simple with negligible computational cost, but ignores individual differences and may not be able to cope with complex evacuation situations [50,56,57]; the third is the Artificial Intelligence-based methods, which can adapt to different conditions and provide accurate predictions, but requires extensive historical data to train the model [58–60]; the forth is the intelligent traffic systems- based method, which can update traffic conditions in real-time, but depends on the operation of specific equipment such as traffic sensors[25,61,62]. These measures and approaches provide a technical and theoretical basis for estimating evacuation times. However, most previous research considered the overall process from a separate perspective or assumed the disaster scenarios to be deterministic or static [63]. Variations in different areas, diverse flood scenarios, and distinct road network characteristics can result in significant differences in evacuation times. Therefore, a more systematic and holistic way to assess evacuation vulnerability and risk, integrating spatial-temporal variations and potential challenges under dynamic hazards, is needed.

In order to provide timely evacuation information and support precise evacuation decision-making, this study provides a methodological framework for evaluating evacuation vulnerability and risk based on the predicted evacuation time, which can be replicated to generate results systematically. First, this research built a predictive model based on the Random Forest to quantify vulnerability, considering both physical factors of the road network and temporal characteristics. Then, the quantified vulnerability is further integrated with time-varying hazards to assess evacuation risk, where a mathematical-based method was used to estimate the evacuation time under the hazard evolution and traffic congestion impacts. The main objective here is to provide quantitative and straightforward evacuation information for both authorities and individuals, including vulnerable times and areas oriented to evacuation preparation, risk distribution oriented to individual evacuation decisions, and regional evacuation deadlines oriented to evacuation notifications. The remainder of this paper begins with a detailed description of the evacuation vulnerability and risk assessment process. Following that, a case study is presented to verify the practicality of the proposed approach for a flooding scenario from the 2015 Kanto-Tohoku heavy rainfall event in Joso City, Japan. The next section contains the results and discussions of the assessment and the corresponding evacuation information provided for individuals and local authorities. Conclusions and future works follow these sections.

2. Evacuation vulnerability and risk assessment process

This study focused on the quantitative assessment of evacuation vulnerability and risk under dynamic flooding hazards. The methodology implemented has the following sequence: 1) The travel time prediction model, which allowed the estimation of the travel time under ideal evacuation conditions considering multiple spatial and temporal characteristics; 2) The evacuation vulnerability assessment depending on the predicted travel time on the shortest evacuation route; 3) The individual evacuation risk assessment and regional evacuation deadline determination according to the evacuation necessity, ability (passable evacuation route for driving and walking), and difficulty (increased evacuation time) under flooding hazard and traffic congestion impacts.

2.1 Evacuation time prediction model development

According to previous research, most people would choose a private vehicle during self-evacuation [64,65]. Therefore, this study developed a prediction model to estimate the ideal vehicle evacuation time along each evacuation route. In our previous study, we used spatial characteristics on the road as input variables and applied a classification algorithm to estimate evacuation time, which is straightforward but has low accuracy and is limited in reflecting the time-varying characteristics [66].

Herein, this paper proposed a new approach and two improvements on model inputs and output to address the remaining problem. The new approach is to utilize the Random Forest (RF) Regression Model developed by Brieiman [67], to predict evacuation times along different evacuation routes. The main reason for this selection was its excellent performance, high robustness, high accuracy, and short calculation time compared with other machine learning methods [68,69]. The RF model combines two powerful machine-learning techniques: the Bootstrap Aggregating (Bagging) method introduced by Breiman and the random feature selection method introduced by Ho, Amit and Geman [60,67,70–73]. The model not only effectively increases the selection randomness in features and training samples, but it also improves accuracy and reduces overfitting without significantly increasing computation complexity [59,74,75]. Accordingly, the Random Regression Algorithm has been extensively applied in various regression analyses in transport, including the prediction of travel time and traffic flows [59,68,69]. These studies have verified the practicability and effectiveness of the algorithm. Herein, the model assumes that S is a training set with size $N \times M$, where N represents the number of data, and M represents the number of variables. The prediction process based on the RF model is presented as follows:

Step1: Set the number of decision trees as K and the depth as d.

Step2: Use the bootstrap aggregating (bagging) method to generate K data subsets with size $N \times M$: $D = \{D_1, D_2, D_3, \ldots, D_K\}$.

Step3: For each D_i ($i<=K$), use the random features selection method to randomly select m ($m<M$) features then generate variable subsets: $V_i = \{V_1, V_2, V_3, \ldots, V_m\}$.

Step4: Apply the CART method to construct the decision tree $f_i(D_i, V_i)$ by partitioning the dataset into multiple subsets. For each partition node, the optimal partition feature j and the optimal partition location q satisfying the following equation are found to ensure data within each subset belongs to the same class.

$$\min_{j,q}[\min \sum_{x_i \in \mathrm{R}_1(j,q)} (y_i - c_1)^2 + \min \sum_{x_i \in \mathrm{R}_2(j,q)} (y_i - c_2)^2 \tag{1}$$

$$\mathrm{R}_1(j,q) = \{x|x^{(j)} \leq q\},\ \mathrm{R}_2(j,q) = \{x|x^{(j)} > q\} \tag{2}$$

$$\mathrm{c_m} = \frac{1}{\mathrm{N_m}} \sum_{x_i \in \mathrm{R_m}(j,q)} y_i\,, \qquad x \in \mathrm{R_m}\,, m = 1,2 \tag{3}$$

Where $R_1(j,q),\ R_2(j,q)$ are the two subsets partitioned by j and q; c_m, N_m are the mean value and data number in $R_m(j,q)$; x_i, y_i are input and output variables of data *i*. The $f_i(D_i, V_i)$ will continuously grow until its depth reaches *d*. The dataset is thus partitioned into *P* subsets $\{R_1, R_2, R_3..., R_P\}$ and the output is denoted as follow:

$$f_i(\mathrm{D_i}, \mathrm{V_i}) = \emptyset_{\mathrm{D_i},\mathrm{V_i}}(X) = \sum_{p=1}^{P} \mathrm{c_P} * \mathrm{I_{R_P}}\ (\mathrm{X}) \ \ (\mathrm{I_{R_P}}\ (\mathrm{X}): indicator\ function) \tag{4}$$

$$\mathrm{I_{R_P}}\ (\mathrm{X}) = \begin{cases} 1, & if\ X \in \mathrm{R_P} \\ 0, & if\ X \notin \mathrm{R_P} \end{cases} \tag{5}$$

Step5: Calculate the average output of all decision trees as the final prediction result.

$$f(S, M) = \emptyset_{S,M}(X) = \frac{1}{K} \sum_{i=1}^{K} \emptyset_{\mathrm{D_i},\mathrm{V_i}}(X) \tag{6}$$

The first improvement is to modify model input by incorporating road attributes with time properties, considering the significant impact of spatial and temporal features on travel time [74,76,77]. This approach resulted in 11 input variables for the prediction model, including four road geometric variables, one land use variable, four intersection variables, and two temporal variables, as indicated in Table 1. To present the variables' effect on evacuation time more accurately, the variables of road geometric and land use were further classified into different levels according to their characteristics (Table 1).

The second improvement is to modify model output as travel speed based on the one-to-one correspondence between travel time and speed [78,79]. The travel speed was calculated by dividing the collected route length by the travel time. Then, this research developed Model 1, Model 2, and Model 3 to compare the performance of these two improvements with the new approach. Model 1 used the RF model with previous inputs and output; Model 2 improved the model inputs; Model 3 improved both model inputs and output. As shown in Table 1, the evacuation time and speed along the evacuation route *i* at time *t* are the outputs of Model 1,2 and Model 3, respectively. The remaining rows are input variables of these three models, including the related spatial variables on route *i* of Model 1 and the added temporal variables at time *t* of Model 2, 3.

Table 1 Variable Description of RF Model

S	Definition	Type
T	Evacuation time along evacuation route *i* at time *t*	Output of model1,2
V	Evacuation speed along evacuation route *i* at time *t*	Output of mode 3
L	Length of the route *i*	Input road geometric variables
W1-W5	Length percentage of different road width (*W1*: over 19.5m, *W2*:13m~19.5m, W3:5.5m~13m, W4:3m~5.5m, *W5:* under 3m)	
S1-S7	Length percentage of different road slope (*S1*: under -9%, *S2:* -9%~-7%, *S3:* -7%~-5%, *S4*: -5%~5%, *S5*: 5%~7%, *S6*:7%~9%, *S7*: over 9%)	
R1- R4	Length percentage of different road curvature radius (*R1*: 0~15m, *R2*: 15~60m, *R3*: 60~150m, *R4*: 150m~)	
Z1- Z2	Length percentage of road within different zones (*Z1*: Agriculture zone, *Z2*: Forest zone)	Input land use variables
IS	Number of straight ahead at intersections	Input intersection variables
IL	Number of left turns at intersections	
IR	Number of right turns at intersections	
Sig	Number of signalized intersections	
TOD	Time of day (0~23, represent 0am~23pm)	Input temporal variables
DOW	Day of week (1~7, represent Monday ~ Sunday)	

To rigorously evaluate the prediction accuracy of the proposed model, this research applied the Root Mean Square Error (RMSE) and the Mean Absolute Percentage Error (MAPE), which can reflect the average relationship between actual and predicted values. The RMSE measures the average magnitude of the prediction error, whereas the MAPE represents the average ratio of the absolute error to the actual value [69,80]. This research also analyzed the distribution of the Absolute Prediction Time Error (APTE) to assess overall prediction performance, the three indices are calculated as follow:

$$RMSE = \sqrt{\frac{1}{n-1} \times \sum_{i=1}^{n} \left((y_i^{real} - y_i^{pre})^2 \right)} \tag{7}$$

$$MAPE = \frac{1}{n} \sum_{i=1}^{n} \frac{\left| (y_i^{real} - y_i^{pre}) \right| \times 100\%}{y_i^{real}} \tag{8}$$

$$APTE = \left\{ error \middle| error = \left| (y_i^{real} - y_i^{pre}) \right| \right\} \tag{9}$$

Where, y_i^{real} and y_i^{pre} represent the actual and predicted values of evacuation travel time; *n* represents the number of measurements.

2.2 Evacuation vulnerability assessment process

In an emergency, the shortest route to the nearest evacuation shelter is usually the evacuees' first choice and reaction [81]. Thus, this research quantified the evacuation vulnerability of each building by predicting the travel time along its shortest evacuation route. Herein, Dijkstra's Algorithm, a graph search algorithm, was used to find the shortest route and the nearest shelter. Dijkstra's algorithm was conceived by the Dutch computer scientist Edsger Dijkstra in 1956 and published in 1959. This algorithm is one of the most known methods in shortest-path finding and has been widely applied in emergency evacuation planning due to its clarity and simplicity [82–86].

Herein, the road network was defined as a directed graph G (V, E) to adapt this algorithm. The vertices V represented the road intersections, and the edge E_{ij} denoted the road connecting two neighboring vertices V_i, V_j with a length of L_{ij}. Here, the target is to find the shortest evacuation route to shelters for each building. Therefore, the Dijkstra's Algorithm was run multiple times for every origin building V_O, with each shelter tagged as the destination V_D, until finding the shortest evacuation routes S_{OD} to all shelters. The route with the minimum distance was regarded as the shortest evacuation route S_O; the corresponding shelter was the nearest, while the remaining shelters were optional. Then, the evacuation time on S_O was estimated by the proposed model in Section 2.1 to quantify the evacuation vulnerability, which can reflect the ideal evacuation time when the hazard did not occur. In addition, to further reveal the regional evacuation vulnerability distribution, the Kriging Interpolation Method was applied to output the equivalent surface of evacuation vulnerability based on the discrete buildings' vulnerability data. The output of regional vulnerability was then visualized in ArcGIS.

2.3 Evacuation risk assessment process

When people evacuate in an emergency scenario in the real world, there are multiple potential challenges that evacuees may face during an ongoing hazard. These challenges can result in longer evacuation times or even the inability to evacuate. In such situations, the evacuation time may differ from normal traffic time in the road network. Therefore, this research further estimated the evacuation time by considering the impact of potential challenges that may occur during an evacuation, including hazard evolution on route detours and traffic congestion on time delay. Then, evacuation necessity, evacuation ability (passable evacuation route for driving and walking), and evacuation difficulty (increased evacuation time) were introduced to quantify the time-varying individual evacuation risk under dynamic hazards. Following that, the regional evacuation deadline was further determined to specify regional evacuation priority to ensure timely implementation of evacuation.

2.3.1 Evacuation route determination under hazard evolution

In an emergency evacuation, the shortest passable route S_O is not always optimal under time-varying hazards and population concentration impacts, which may sometimes be impassable or congested [81]. Moreover, evacuees may choose various evacuation routes based on their experience, subconsciousness, road safety, and traffic jams. In this condition, finding passable potential evacuation routes for all buildings in real time requires much computational effort and time under dynamic hazard evolution. As this study aims to reflect the dynamic risk under various scenarios, the quick and precise determination of evacuation routes is needed. Accordingly, as Figure 1 shows, this study proposed a 4-step framework to determine the evacuation route under time-varying flooding scenarios more realistically.

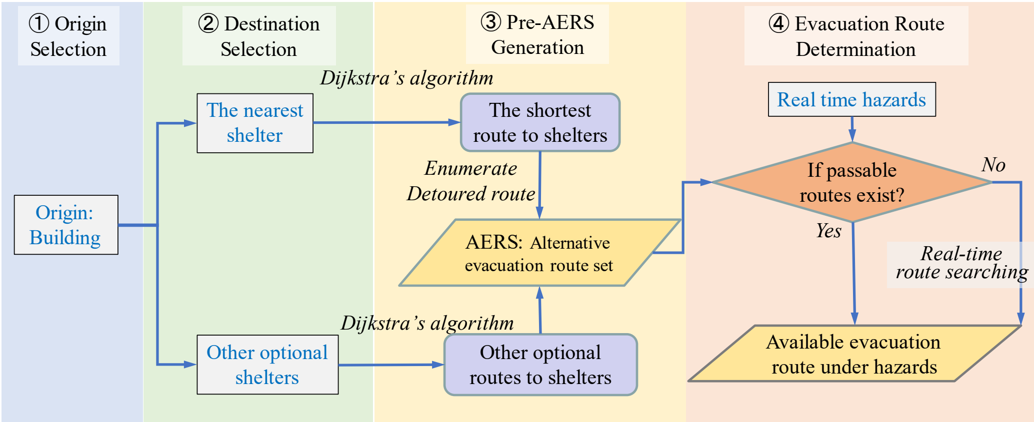

Figure 1 Evacuation route determination under dynamic hazards

In order to find more passable potential routes under dynamic flood impacts as soon as possible, this study generated the Alternative Evacuation Route Set (AERS) in advance, which consisted of potential evacuation routes to shelters. When flooding occurs, the available evacuation route will be determined considering dynamic flooding impacts as follows: (1) The shortest route S_O and all routes in AERS will overlap with the inundated area to select the passable route; (2) If all pre-generated routes are impassable, real-time route planning will be considered to determine the final evacuation route.

Regarding the pre-AERS generation, although in a continuous space-to-plane geometry, infinite routes exist between two locations. Nevertheless, in an emergency evacuation scenario, evacuees do not decide the route forward at each step. Generally, they follow their first choice and only change their movement direction under specific conditions [81,87,88]. Accordingly, this research enumerated the possible inundation conditions on the shortest evacuation route from each building to its nearest shelter selected in Section 2.2. Then, the rerouted evacuation routes to avoid inundation areas were predetermined by using Dijkstra's Algorithm. It is worth mentioning that evacuation routes to other optional shelters were also considered in AERS. If the rerouted detour route to the nearest shelter was farther than to optional shelters, the evacuation to other optional shelters was considered instead of continuing the detour. The detailed process of pre-AERS generation is as follows:

Step1: Define the shortest evacuation route S_O as a directed graph g (V, E) with $(m+1)$ vertices and m edge (Figure 2.a), then initialize the AERS with S_O and the shortest evacuation route to each optional shelter.

Step2: Generate possible inundation conditions on g (V, E) by enumerating inundated road I_k from edge E_1 to E_m and range the inundated route number n from 1 to $(m\text{-}1)$.

Step3: For each inundated condition I_{edge}, apply Dijkstra's Algorithm to reroute the inundated part (I_k~I_{k+n}) to avoid flooding impact. It is worth mentioning that the route outside the inundation area remains unchanged (Figure 2.b).

Step4: Take the shortest distance to optional shelters as the distance limit, then select the rerouted evacuation route and update the AERS.

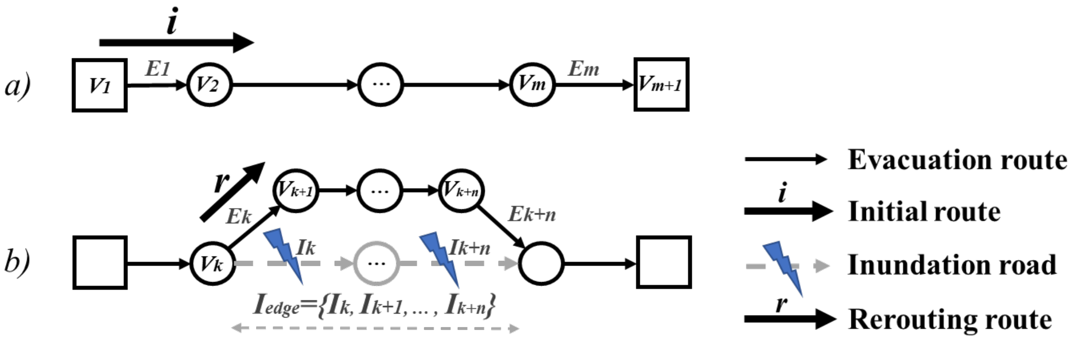

Figure 2 Representation of rerouting evacuation route

2.3.2 Evacuation time estimation under congestion impact

In an emergency scenario, crowding on roads due to population concentration is considered a major obstacle, which may result in delayed evacuation [89]. Therefore, to better estimate the evacuation time, this research first applied the RF model in section 2.1 to predict the ideal time on each available evacuation route. Then, the congestion resultant evacuation time was further estimated in this section.

According to previous research, the primary determinant of congestion is "travel demand", and the interplay of its corresponding traffic volume and road capacity (the maximum hourly flow rate that can occur without queues developing) determines the traffic congestion level [90]. Therefore, to estimate the congestion resultant evacuation time, it is necessary to clarify the relationship between the traffic volume and road capacity during evacuation. Considering selecting the shortest route is the individual's first choice, and there are few opportunities to deviate from the initial path after the evacuee determines an evacuation route [54,81]. This research assigned vehicles to the shortest evacuation route for all origin buildings and destination shelters (O-Ds) pairs. Then, the O-Ds were used to calculate the total evacuation volumes V_e along each road segment e, which is the sum of all flows from all paths that pass through it as follows.

$$V_e = \sum_{o,d} f_s^{od}\, \delta(s,e) \tag{12}$$

$$VC_e = \frac{V_e}{C_e} \tag{13}$$

Where f_s^{od} is the flow between the origin o and destination d on route s, $\delta(s,e)$ =1 if road segment e lies on route s, and 0 otherwise. Then, the calculated evacuation volumes V_e were compared with its capacity C_e to derive the VC_e ratio, reflecting how successfully a road segment can cope with the assigned volume of vehicles. The road capacity was determined using the Highway Capacity Manual based on the area type, where roads in the CBD and other area were set at 1,600 pcu/h/lane and 1700 pcu/h/lane, respectively. Additionally, the capacity of two-lane roads was set at the typical value of 2,200 pcu/h according to the Traffic Capacity of Roads in Japan [91]. If the VC_e is less than or equal to 1, there is no significant delay. Where it is greater than 1.0, it indicates that the flow on the segment exceeds its capacity and will be congested [57,90,92].

In most traffic delay estimation methods, the effect of the VC ratio on travel times is specified by means of the volume-delay function, of which the most widely used are the Bureau of Public Roads (BPR) functions [93,94]. Accordingly, after identifying the VC_e value of each road segment *e*, this research followed the classical BPR function to quantify the congestion resultant evacuation time as follows [93–95].

$$T_e(V_e) = t_e * [1 + \alpha(VC_e)^{\beta}] \tag{14}$$

Where t_e is the normal travel time on road *e*; VC_e is the congestion level, and $T_e(V_e)$ is the congestion resultant evacuation time on road *e* under traffic volume V_e; The parameters α and β in the BPR function are chosen following the government manual based on road type and free-flow speed [94,96].

2.3.3 Evacuation risk assessment process

To evaluate the time-varying evacuation risk under different scenarios, the evacuation necessity, ability, and difficulty were determined separately for each building under the flooding scenario. Since the evacuation preparation information in Japan is usually issued two hours before the evacuation notifications, this research judged the evacuation necessity based on the predicted inundation from the current moment to the next two hours [97]. A building is considered in need of evacuation when it complies with the following conditions: 1) The building would be affected by flooding or lose access to shelters within two hours; 2) The building floors do not satisfy safe vertical evacuation. Herein, the risk value for buildings not requiring evacuation is set to *nan*.

Then, to clarify the evacuation ability of each building, this research overlapped the road network with the inundation data to determine the evacuation route. If there were no passable routes for walking and driving from one building to the shelters, the building was considered to have the highest risk: no evacuation ability. Next, regarding the buildings with evacuation ability, this research estimated their evacuation difficulty according to the estimated congestion resultant evacuation time along each passable route. Herein, the relationship between these times and the available time until losing evacuation ability was considered to reflect the evacuation difficulty to a certain extent. The evaluation function $Risk_i(t)$ describes the evacuation risk from building *i* at time *t*, and its value is the minimum among all passable evacuation routes for walking and driving. For building *i*, a higher *Risk* value means less likelihood of being safely evacuated. The evacuation risk at time *t* is defined as follows:

$$Risk_i(t) = \begin{cases} nan, & no\ evacuation\ necessity \\ \text{inf}, & no\ evacuation\ ability \\ \min\limits_{n,m}(Risk_i(r,t) = \min\limits_{n,m}\left(\dfrac{T_i(r,t)}{A_i(t)}\right), & else \end{cases} \tag{15}$$

Where *n* is the number of passable evacuation routes, *m* is the available transport mode, including walking and driving. $Risk_i(r,t)$ is the evacuation risk along passable evacuation route *r* from building *i*. $T_i(r,t)$ denotes the congestion resultant evacuation time along route *r* at time *t*. Here, the driving time was estimated following section 2.3.2, and roads flooded to a depth of over 30cm were considered impassable for driving [98,99]. Since the walking speed decreases with increasing inundated depth, this study calculated the walking time based on a certain speed of 0.83m/s for 0~30cm and 0.68m/s for 30~70cm, according to Bernardini's research [100,101]. Walking speed on roads without inundation was set at 1.36m/s (adult average walking speed in Japan [102]), whereas roads inundated by more than 70 cm were considered impassable for walking [103,104]. $A_i(t)$ denotes the available evacuation time at time *t*, the specific calculation is as follows:

$$A_i(t) = \min\{2hour, (t_{i,inf} - t)\} \tag{16}$$

Where $t_{i,inf}, t$ refers to the time building *i* loses its evacuation ability and the current time, respectively. For buildings that will not lose their evacuation ability within 2 hours, the available evacuation time will be defined as 2 hours. As previously mentioned, the evacuation function describes the evacuation risk of each building. $Risk_i(t)$ measures how difficult it is for evacuees to reach shelters. When the required evacuation time on passable routes increases or the available time decreases, the evacuation risk will increase, and evacuation from the building becomes more difficult. A *RISK* value greater than 1.0 indicates that the needed evacuation time exceeds the available time and that the evacuation would be extremely dangerous. Correspondingly, when there is no passable route, the evacuation risk will increase to infinity.

In addition, to prevent irreversible dilemmas due to the inability evacuation, this research further estimated the regional evacuation deadline ED_z oriented to authorities' evacuation notifications, which concerning the appearance time of no evacuation ability buildings and the longest required evacuation time from buildings to shelters as follow:

$$ED_z = Time_{z,inf} - \max(T_{z,i}) \tag{17}$$

Where z denotes the regional zone z, $Time_{z,inf}$ and $\max(T_{z,i})$ are the appearance time of no evacuation ability buildings, and the longest required evacuation time arriving at a shelter for buildings within zone *z* before $Time_{z,inf}$, respectively.

3. Case study: Joso, Japan

3.1 Study area and scenario setting

This research chose Joso city in the southwestern Ibaraki prefecture of Japan (Figure 3) as the study area to evaluate the proposed approach. Joso city has an estimated population of 59,969 distributed over a total area of 123.64 square kilometers. There are two major rivers, the Kinu river (the middle river in Figure 3) and the Kokai river (the east river in Figure 3), flowing from the north to the south in Joso. In 2015, this city was severely affected during the Kanto-Tohoku Heavy Rainfall Event. All the floodplain between the two rivers was inundated, and the flood continuously affected 40 square kilometers around [105–107]. Including this event, the Kinu River has caused eight major floods since the 1930s [106]. Therefore, it is worthwhile to evaluate the evacuation vulnerability and risk in this flood disaster-prone city, to make appropriate evacuation decisions and reduce casualties before the onset of, during, or after a hazardous event.

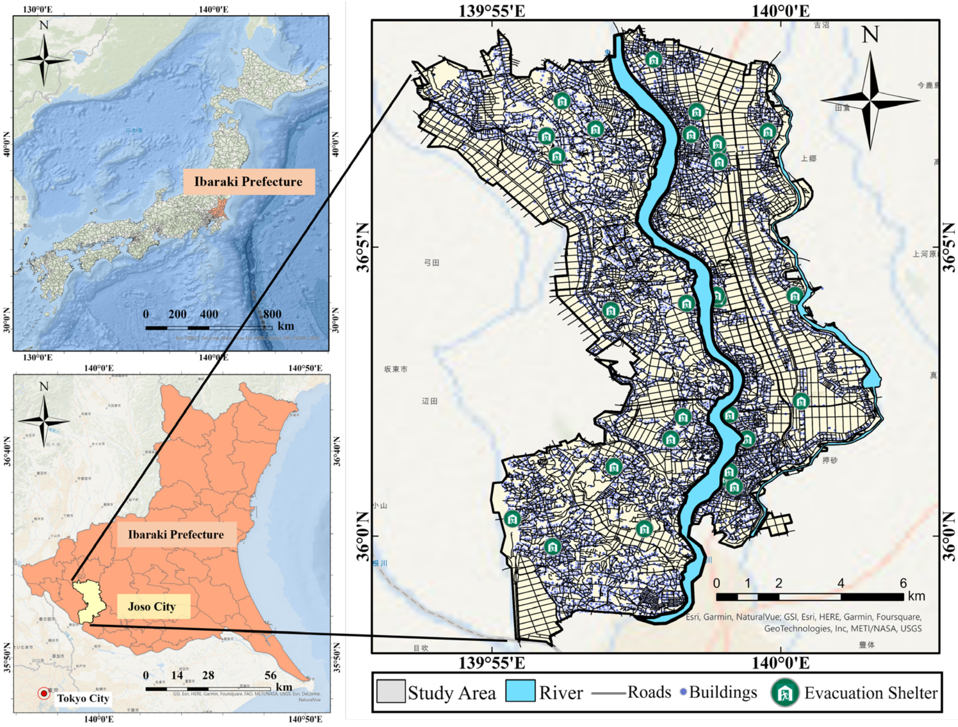

Figure 3 Location of study area

The above-mentioned catastrophic river flooding that occurred in Joso on September 10, 2015, was selected as a case scenario to verify the practicality of the proposed approach. The time-varying inundation data from 00:00 to 17:50 was used to quantify dynamic hazards. Herein, the dynamic inundation was assumed to be forecasted 6 hours ahead and updated at 10-minute intervals. Throughout this process, the risk assessment is updated concurrently with each dynamic hazard update. The corresponding inundation area data divided the study area into 48637 meshes with a size of 50 m*50 m. For each mesh, there were three inundation levels: Less than 30 cm (Level 1), Less than 70 cm (Level 2), and Over 70 cm (Level 3). Herein, the inundation data was obtained by using the Rainfall-Runoff-Inundation (RRL) model, developed by the International Centre for Water Hazard and Risk Management (ICHARM) under the auspices of UNESCO [108]. It is highlighted that the purpose of this paper is not the flood inundation prediction, but the evacuation vulnerability and risk assessment based on the prediction results provided by the mature inundation prediction model.

3.2 Data preparation

The major data types used in this study included location data of evacuation shelters, buildings, signalized intersections, road network data, land use data, and travel time data. Due to the lack of actual traffic data during disaster evacuations, we utilized 231 routes between evacuation shelters and collected their normal daily travel time data to calibrate the prediction model. The travel time data of these 231 routes were collected from the Google Maps distance matrix (API) from November 18 to November 24, 2021, with a 1-hour collection interval. The collected data included 38808 records, and each record consisted of origin and destination locations, access point locations, travel distance, and travel time.

The location data of buildings and evacuation shelters were collected from the Micro Geodata Forum and the official website of Joso City, respectively [109,110]. The road network, land use, and other related data were all downloaded from the Geospatial Information Authority of Japan (GSI). The GSI is a national organization that conducts national surveying and mapping activities in Japan [111]. The collected data contained 24054 road segments in the road network and 151 signalized intersections in Joso City. Then, ESRI ArcGIS Pro 3.0 was used for data preprocessing to obtain road information (e.g., road length, width, curvature radius, slope) for the evacuation time prediction model.

4. Results and discussion

4.1 Verification of the evacuation time prediction model

In this section, the collected travel time data, and the corresponding road information on 231 routes were used to build and verify the evacuation time prediction model. The collected dataset was divided randomly into 80% and 20% for training and testing, respectively. The train-test procedure was repeated 500 times to ensure the accuracy of the results. Table 2 shows the average prediction results from 500 random replicate runs. Where Model 1 used the RF model with previous inputs and output; Model 2 improved the model inputs; Model 3 improved both model inputs and output. As indicated, both Model 2 and Model 3 outperformed Model 1, had about 99.9% APTE distributed within five minutes. Considering that most of the disaster information referred to during the evacuation decision process is updated every five or ten minutes [112–114], the performances of both Model 2 and Model 3 are acceptable in this research. Furthermore, as shown in Table 2, Model 3 outperformed Model 2 on all verification criteria, including an RMSE of 0.88 min, a MAPE of 5.88%, and 99.92% APTE distributed within five minutes. The high accuracy obtained demonstrated its ability to handle complex interactions among input variables and generate reasonable evacuation time predictions.

Table 2 Performance of the evacuation time prediction model

Prediction accuracy	RMSE (min)	MAPE (%)	APTE distribution (%) 1 min	2 min	3min	4 min	5 min
Model 1	9.67	69.1	9.35	16.95	24.65	31.18	38.57
Model 2	1.10	7.19	68.18	92.54	98.63	99.73	99.90
Model 3	0.88	5.88	79.74	96.97	99.07	99.82	99.92

Figure 4 illustrates seven days' prediction results for a better understanding of these three models, where the horizontal axis reflects the change of time, and the vertical axis is the average travel time of all testing routes under each specified time. The red line represents the collected value, while the blue, gray and black lines represent the predicted results from Model 1, Model 2 and Model 3, respectively. To comprehensively clarify the performance of these three models, this research further compared the error distribution for all testing roads across the three models in Figure 5. The vertical axis is the deviation between prediction and actual values, where the blue, red, and green points represent the deviations of Model 1, Model 2, and Model 3, respectively. As shown in Figure 4 and Figure 5, both Model 2 and Model 3 accurately predicted the overall trend of evacuation time, whereas model 3 performed better in predicting evacuation time under various temporal characteristics. As a result, we conclude that Model 3, which incorporates the effect of temporal and spatial characteristics on travel speed, best suits this research.

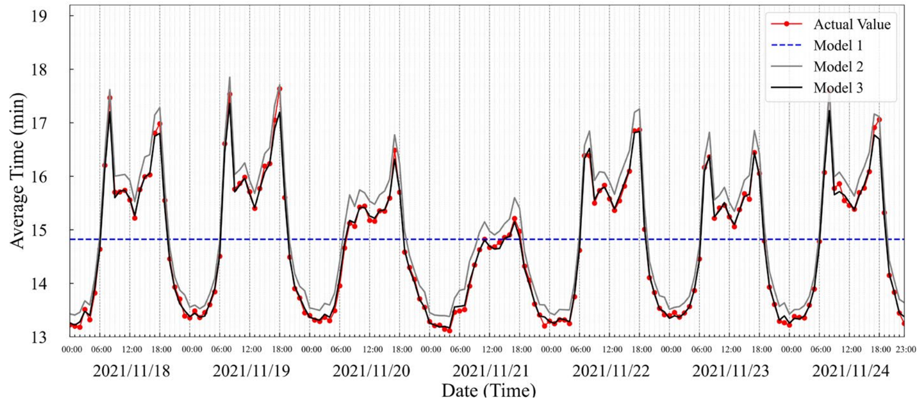

Figure 4 Average prediction results of Model 1, Model 2 and Model 3

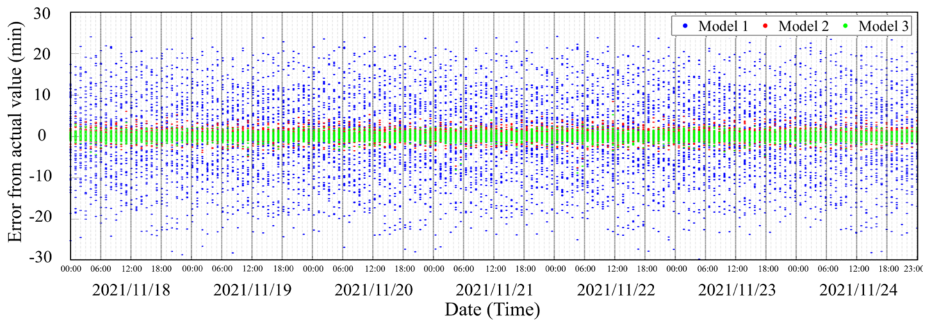

Figure 5 Sample prediction results of Model 1, Model 2 and Model 3

4.2 Evacuation vulnerability assessment based on ideal evacuation time

4.2.1 Evacuation vulnerability assessment from a temporal perspective

Figure 6 compares the statistic of the ideal evacuation time for all buildings during the given scenario from a temporal perspective. It can be seen that most buildings, with an average of 96.66% (50031 of the total 51757), had an ideal evacuation time of fewer than six minutes during the 18 hours. The longest ideal evacuation time among them is at 17:00, with 9.22 minutes. In this situation, under ideal pre-disaster evacuation conditions, all buildings can be safely evacuated within 10 min.

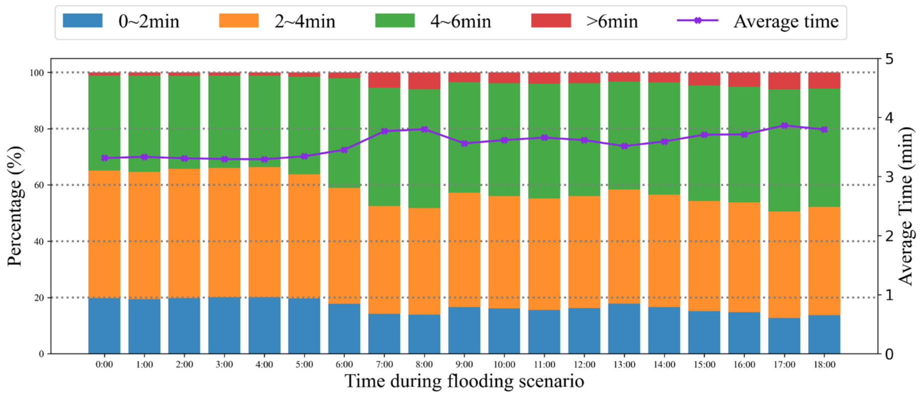

Figure 6 Temporal distribution of the ideal evacuation time during the flooding scenario

On the other hand, the ideal evacuation time between 7:00~8:00 and 17:00~18:00 is longer than the other times. An average of 6.31% of buildings require more than 6 minutes to evacuate during these times. The main reason for a long time was that these are peak commute hours when traffic volumes are higher, and traffic jams are common. It should be noted that traffic congestion is more likely to occur if the evacuation is carried out during these times. As a result, these critical times require extra caution, where evacuation, traffic management strategies should be prepared in advance to avoid other consequences such as traffic congestion.

4.2.2 Evacuation vulnerability assessment from a spatial perspective

Based on the buildings' location and their corresponding evacuation vulnerability, the spatial distribution of regional vulnerability can be obtained using GIS tools. Figure 7 illustrates the regional vulnerability assessment results at 00:00, 06:00, 12:00, and 18:00 on September 10 from a spatial perspective, different colors represent the accessible areas within different times. Only these scenarios are shown because there are no discernible changes in a short period. As indicated, the evacuees in the high-vulnerability buildings represented in black would take over 6 minutes to reach their nearest evacuation shelter. It can be seen from Figure 7 that these buildings are primarily distributed around Yuki-bando-road (Northwest of the study area), Aguri-road (central-north of the study area), and Sakura-road (Southeast of the study area). This distribution indicates that these areas are more vulnerable to evacuation under flooding, and it would take longer to reach the nearest evacuation shelter. In this situation, it is more necessary to give special attention and issue evacuation warnings ahead of time for these areas, because keeping safe during evacuation is more difficult for them.

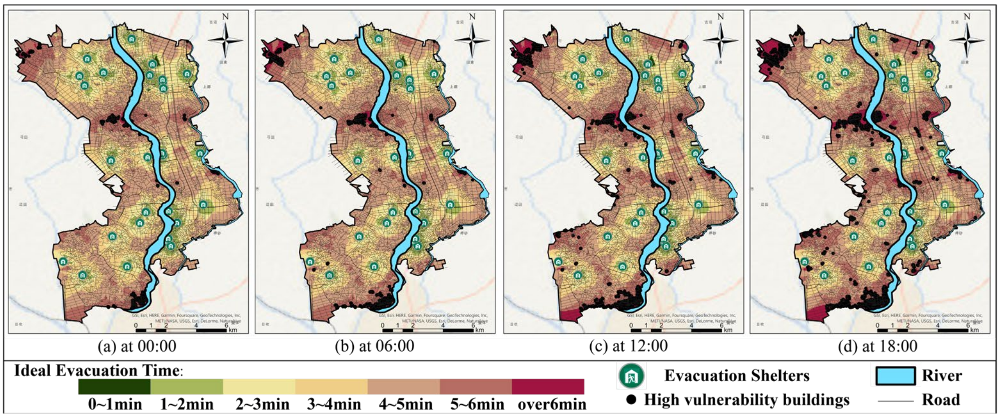

Figure 7 Spatial distribution of the ideal evacuation time during the flooding scenario

Overall, the ideal evacuation time effectively reflected the time-varying evacuation vulnerability, with Dijkstra's Algorithm exploring the shortest evacuation route and the RF model predicting evacuation time by multiple temporal-spatial characteristics. Following that, the estimated vulnerable areas and times provided forth insights into evacuation preparedness about, "When and where need more evacuation preparation?".

4.3 Evacuation risk assessment based on vulnerability and hazards

4.3.1 Identification of affected buildings and roads

To clarify the evacuation necessity, ability, and difficulty of each building, this research overlaid the building's locations and road network with the time-varying inundation area under the given flooding scenario. Figure 8 summarizes the percentage of inundated buildings and roads. As indicated, the overlapping resulted in the identification of 33289 (64.31% of the total) buildings affected by flooding, regardless of the depth. Given the prevalence of low-rise buildings in Japan, this research assumes that one-story buildings are safe from inundation at Level 1, whereas multi-story buildings are safe below Level 2. In this situation, 29963 (90% of the 33289) affected buildings were presumed to require evacuation because it was unsafe to stay home.

Furthermore, as indicated in Figure 8, passable roads continued to dwindle as the flooding progressed. As shown, the increases in roads affected by Levels 1 and 2 were initially sharp and then stabilized at about 5.42% and 19.93%, respectively, at 04:30 and 05:20. On the other hand, the increase in roads affected by Level 3 appeared small at first. However, it continued to increase until 13:50 when the increase rate slowed, and the affected roads stabilized at around 46.18%. As a result, a total of 68.91% roads were eventually affected at 17:50. According to previous research, the maximum passable depths in this research were assumed as 30 cm for driving and 70 cm for walking, respectively [98,99,103,104]. In this situation, the impassable roads for driving and walking reached a maximum of 65.18% and 47.12%, respectively. These continued impacts on roads would result in significant losses, evacuees being unable to move out of the flooded area safely if all surrounding roads are inundated [115].

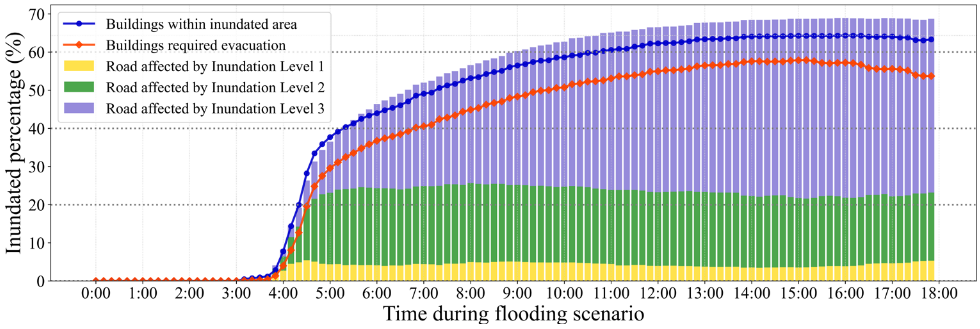

Figure 8 Temporal distribution of inundated buildings and roads

4.3.2 Evacuation risk assessment oriented to individual building

After identifying the inundated buildings and roads, the evacuation necessity, ability, and difficulty were further judged and incorporated in Eq.(15) to assess dynamic individual risk. As previously stated, the evacuation necessity was determined based on the inundation condition within the next two hours. Therefore, this section assessed the evacuation risk at ten-minute intervals from 00:00 to 15:50. A time series was plotted to illustrate the time-varying individual evacuation risk from a temporal perspective, shown in Figure 9. Here, blue indicates no-evacuation-necessity buildings, green indicates no-evacuation-risk buildings, whereas black indicates the highest-evacuation-risk buildings: without evacuation ability. In addition, other buildings were divided into three classifications (corresponding to the green, yellow, and red colors in Figure 9), indicating low-evacuation-risk (where $0 < RISK \leq 0.2$), middle-evacuation-risk (where $0.2 < RISK < 1$), high-evacuation-risk (where $RISK \geq 1$) respectively.

According to the predicted results of inundation evolution, the flooding under the given scenario began at 03:10. As indicated, all buildings are safe from 00:00 to 01:10 (2 hours before flooding). Within 30 minutes of the flooding, 40.16% of buildings required evacuation, where 92.15% of them were deemed to have a low evacuation risk. In the following times, more and more buildings required evacuation as the flooding progressed, while the low-risk buildings also gradually evolved into higher risk. At 15:50, only 40.80% of buildings had no evacuation necessity, and only 6.40% were assessed as low evacuation risk. This change indicates that only about half of the buildings were deemed safe during the entire scenario. However, it must be kept in mind that this research assumed a conservative approach, may result in a slight deviation from reality. On the other hand, the evacuation in this research is assumed to be at risk until the evacuees arrive safely at shelters, even though their lives are no longer threatened once they leave the inundation area.

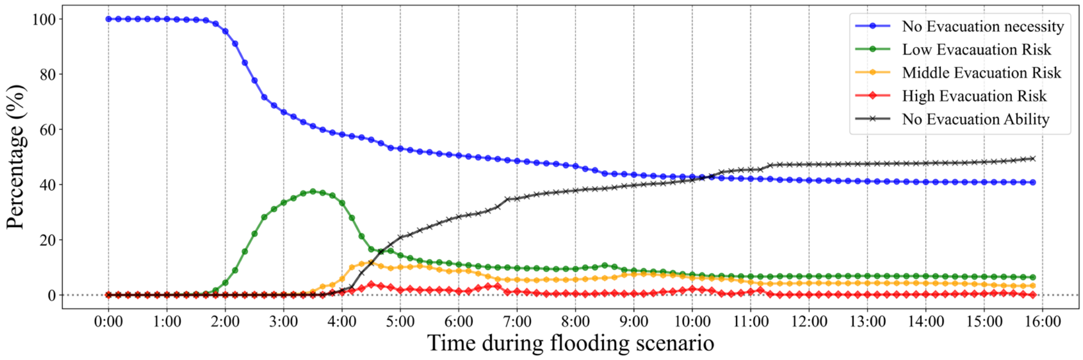

Figure 9 Temporal distribution of evacuation risk during the flooding scenario

In addition, the proportion of buildings without evacuation ability (black color in Figure 9) had remained stable at first, then increased sharply from 03:40 (30 min at flooding) to 05:00 (100 min at flooding) and continued to increase at a slower rate. At 10:20 (7 hours and 10 minutes after the disaster), buildings with no evacuation ability reached 43.02%, surpassing buildings with no evacuation necessity as the highest percentage type. Then, these buildings with no evacuation ability continuously increased to 49.38% at 15:50. In this process, buildings with middle-risk, and high-risk consistently occupied a smaller proportion, with a maximum of 11.86% and 3.83%, respectively. To better understand their evolution, the temporal-spatial distribution of evacuation risk was plotted at specific times in Figure 10.

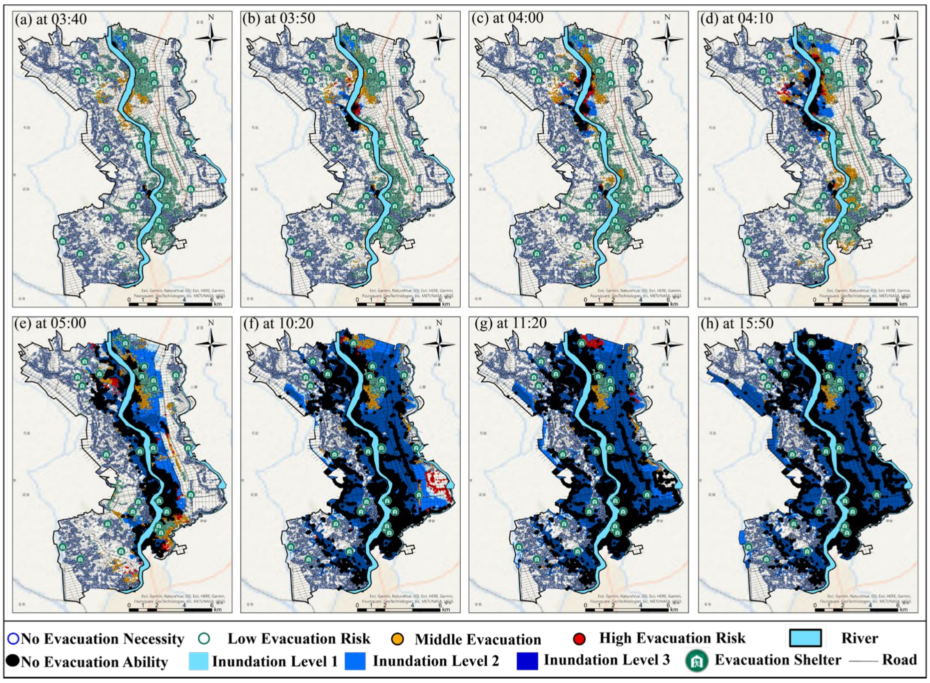

Figure 10 Spatial distribution of evacuation risk during the flooding scenario

As indicated, the no-evacuation ability buildings mainly distributed near the Kinu River. The main reason for the sharply increased from 03:40 was that the inundation area was rapidly expanding and spreading, with both the east and west banks of the river being affected. The ongoing inundation continued to trap buildings (black in Figure 10), making safe evacuation increasingly impossible. Moreover, the distribution of middle risk (orange in Figure 10) and high risk (red in Figure 10) reflect where evacuation difficulties may be encountered, including (1) buildings surrounding the flooded area and (2) buildings whose evacuation routes may be congested. The distribution of these middle-high-risk buildings reveals whether an evacuation can be implemented in time. It also predicts the location of buildings that will lose evacuation ability. Furthermore, it can be found that these buildings at risk do not exactly coincide with the inundated areas. Even if buildings are located in safe areas, evacuation may become hard due to the inundation or congestion of the evacuation routes. Thus, individuals need to keep aware of their time-varying evacuation risk.

Regarding the emergency evacuation for these buildings, it should be stated that the greater the risk value, the earlier the evacuation should begin after evacuation notification. When a building is at high risk, it means that the time required for safely evacuating exceeds the time currently available, evacuation will become very dangerous, and the evacuation route may be impassable at any time. Herein, the increased percentage of buildings without evacuation ability can reach a maximum of 5.11% under the given flooding scenario, resulting in 2643 more buildings being impossible to evacuate every ten minutes. In this situation, the buildings with no evacuation ability deserve the primary concern, followed by high-risk buildings, and the evacuation must be taken as soon as possible to prevent an irreversible situation. In addition, for middle-evacuation-risk buildings, it is also necessary to take earlier emergency evacuation because the situation may quickly deteriorate and even turn into a higher evacuation risk in such a short time under the flooding evolution.

4.3.3 Regional evacuation deadline estimation oriented to authorities

Figure 11 illustrates the accessible area evolution using the elementary school zonation as an example. As shown, various colors correspond to the accessible areas that can be reached within different times from the shelters. Areas without color coverage are inaccessible to shelters by both driving and walking. Buildings in these areas that could not accommodate vertical evacuation were inability to evacuate (black in Figure 11). As indicated, the Kinu River first inundated area in the Tama and Toyooka Elementary school zone (Zone3, Zone10). Then as the flooding inundation spreads, the accessible area in each zone becomes less, and the time required becomes longer.

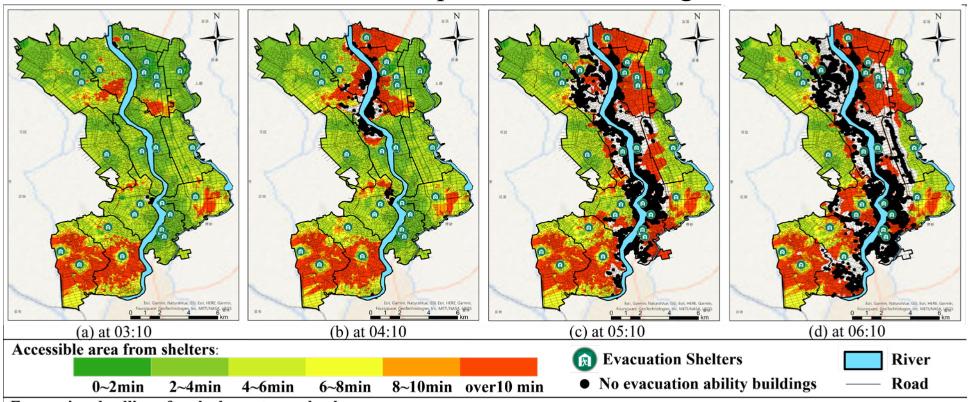

Evacuation deadline of each elementary school zone:

Zone1	Zone2	Zone3	Zone4	Zone5	Zone6	Zone7	Zone8	Zone9	Zone10	Zone11	Zone12	Zone13	Zone14
iinuma	okada	tama	ishige	toyoda	sugahara	ohanawa	mitsuma	goka	toyooka	ono	sugao	kensei	mitsukaido
3:20	3:18	2:55	3:17	3:42	3:41	3:27	3:28	3:55	2:38	3:52	5:25	3:05	3:47

Figure 11 Distribution of regional accessible areas and evacuation deadline

After identifying no evacuation buildings' appearance time and the longest required evacuation time to shelters, Figure 11 further summarizes the evacuation deadline for each elementary school zone. It can be seen that the Toyooka elementary school zone (Zone10) has the earliest evacuation deadline of 02:38, while the Sugao elementary school zone (Zone12) has the latest evacuation deadline of 05:25. There is about 3 hours difference between these two times, in this situation, simultaneous evacuation of the entire region is inappropriate and inefficient. Therefore, this research further specifies the priority of regional evacuation according to the key timing of dynamic hazards and individual evacuation risk (Table 3). In light of these evacuation priorities and deadlines, authorities can develop an appropriate evacuation plan and further issue evacuation notifications to the appropriate zones at the appropriate time.

Table 3 Evacuation priority according to regional evacuation deadline

Evacuation priority	Zones	Evacuation deadline
Primary concern	Zone3, Zone10, Zone13	Before Hazards occurrence
Secondary concern	Zone1, Zone2, Zone4, Zone5, Zone6, Zone7, Zone8, Zone9, Zone11, Zone14	Before or during the sharply increased period of individual evacuation risk
Tertiary concern	Zone12	After sharply increased period

Overall, the proposed risk assessment method explicitly reflected the time-varying individual evacuation risk and regional evacuation deadline under the given flooding scenario. The individual evacuation risk can make the public aware of their situations, answering the question, “Who should be evacuated?”. Furthermore, the regional evacuation deadline can help authorities specify the evacuation priority to ensure timely evacuation, which answers the question, “When should be evacuated?”. Since the individual risk and regional deadlines were predicted two hours in advance, individuals and local authorities can get an accurate picture of the individual risk distribution and regional evacuation priority and subsequently make more scientific judgments.

5. Conclusions and future work

This paper has developed an approach to assess evacuation vulnerability and risk based on evacuation time, with evacuation route-finding by Dijkstra’s algorithm, travel time prediction by Random Forest algorithm, and evacuation time estimation under hazard, traffic congestion impacts. This approach not only assessed evacuation vulnerability concerning the ideal evacuation time prior to flooding, but also integrated the evacuation necessity, ability, and difficulty to quantify individual evacuation risk, as well as regional evacuation deadlines under flooding impacts.

In the present study, this proposed approach was applied to a flood-prone city, Joso, as a case study. The application results demonstrated the approach’s validity and practicality: (1) The prediction model achieved higher accuracy with an RMSE of 0.88min and a MAPE of 5.88% by incorporating temporal-spatial impacts on travel speed. (2) The assessed evacuation vulnerability illustrated the vulnerable areas and times before hazards occurred. (3) The assessed individual risk identified the buildings whose evacuation to shelters may be extended or become impossible. (4) The estimated regional evacuation deadlines specified the evacuation priority under flooding impacts. The information acquired through this research (such as vulnerable areas and vulnerable times, high-risk buildings, and high-evacuation-priority regions) can enable individuals to understand their situation and facilitate awareness to make the right evacuation decisions. On the other hand, for local authorities, state, and federal agencies, this research can support planning precise evacuation strategies, issuing timely evacuation warnings, ensuring prompt protection of resident’s property, and reducing casualties during hazard and emergency evacuation.

Given that local authorities are often the first responders to emergencies, this vulnerability assessment method can help them identify the areas vulnerable to disaster evacuation and take targeted measures such as signage enhancements, community awareness campaigns, or developing localized emergency response plans. When a disaster occurs, this risk assessment can help them monitor the individual risk and regional evacuation deadline at any time. Once risk levels rise, they can respond quickly to issue evacuation notifications and initiate evacuation plans. Moreover, it can also guide urban and regional planning for state and federal agencies, such as informing land use, infrastructure development, allocating resources judiciously, and prioritizing the development and maintenance of efficient evacuation routes. Such integration can empower local authorities and higher-level agencies to fortify disaster preparedness and response capabilities.

This straightforward approach can be used as an efficient, practical tool and reproduced worldwide. The results can provide individuals and authorities with quantitative and visualized information for evacuation preparations and decision-making. Still, the current approach may be expanded and improved in some ways. The scope of future work and challenges for this study includes the following extensions:

(1) Applying the proposed approach in multiple cities (e.g., vulnerability and risk assessment in flood prone city). The proposed methodology framework has a high degree of generalizability. However, when constructing the travel time prediction model, this study used the data from Joso city as a training sample, resulting in a model oriented to this specific city. The future challenge is integrating diverse data sources more comprehensively and building a multi-city-oriented travel time prediction model, which can extract and adapt to different cities' travel characteristics.

(2) Accounting for the effects of dynamic population in the evacuation process. This study regarded each building as the evacuation origin to estimate the vulnerability and risk of traveling from buildings to shelters. As the actual evacuation may be more complicated, the future challenge is how to consider the evacuation demands of the dynamic flow on the road network, and the various evacuation characteristics among different population groups (e.g., evacuation speeds for different ages and genders).

Acknowledgements

This work was supported by Council for Science, Technology and Innovation (CSTI), Cross-ministerial Strategic Innovation Promotion Program (SIP), Enhancement of National Resilience against Natural Disasters (Funding agency: National Research Institute for Earth Science and Disaster Resilience), and JST SPRING, Grant Number JPMJSP2136.

Reference

[1] J. Rentschler, M. Salhab, B.A. Jafino, Flood exposure and poverty in 188 c ountries, Nat Commun. 13 (2022) 3527. https://doi.org/10.1038/s41467-022-30727-4.

[2] J.C.J.H. Aerts, W.J. Botzen, K.C. Clarke, S.L. Cutter, J.W. Hall, B. Merz, E. Michel-Kerjan, J. Mysiak, S. Surminski, H. Kunreuther, Integrating human behav iour dynamics into flood disaster risk assessment, Nat Clim Change. 8 (2018) 19 3–199. https://doi.org/10.1038/s41558-018-0085-1.

[3] M. Wahlstrom, D. Guha-Sapir, others, The human cost of weather-related dis asters 1995–2015, Geneva, Switzerland: UNISDR. (2015).

[4] J.D. Woodruff, J.L. Irish, S.J. Camargo, Coastal flooding by tropical cyclone s and sea-level rise, Nature. 504 (2013) 44–52. https://doi.org/10.1038/nature1285 5.

[5] Y. Hirabayashi, R. Mahendran, S. Koirala, L. Konoshima, D. Yamazaki, S. Watanabe, H. Kim, S. Kanae, Global flood risk under climate change, Nat Clim Change. 3 (2013) 816–821. https://doi.org/10.1038/nclimate1911.
[6] J.H. Christensen, O.B. Christensen, Severe summertime flooding in Europe, Nature. 421 (2003) 805–806. https://doi.org/10.1038/421805a.
[7] H. Alifu, Y. Hirabayashi, Y. Imada, H. Shiogama, Enhancement of river flo oding due to global warming, Sci Rep. 12 (2022) 20687. https://doi.org/10.1038/s41598-022-25182-6.
[8] L. Lin, C. Tang, Q. Liang, Z. Wu, X. Wang, S. Zhao, Rapid urban flood ri sk mapping for data-scarce environments using social sensing and region-stable d eep neural network, J Hydrol. 617 (2023) 128758. https://doi.org/10.1016/j.jhydrol.2022.128758.
[9] H.R. Pourghasemi, A. Gayen, M. Panahi, F. Rezaie, T. Blaschke, Multi-haza rd probability assessment and mapping in Iran, Science of The Total Environmen t. 692 (2019) 556–571. https://doi.org/10.1016/j.scitotenv.2019.07.203.
[10] O. Hosseini, M. Maghrebi, M.F. Maghrebi, Determining optimum staged-eva cuation schedule considering total evacuation time, congestion severity and fire th reats, Saf Sci. 139 (2021) 105211. https://doi.org/10.1016/j.ssci.2021.105211.
[11] P. Lin, S.M. Lo, H.C. Huang, K.K. Yuen, On the use of multi-stage time-v arying quickest time approach for optimization of evacuation planning, Fire Saf J. 43 (2008) 282–290. https://doi.org/10.1016/j.firesaf.2007.08.005.
[12] W. Gai, Y. Du, Y. Deng, Evacuation risk assessment of regional evacuation for major accidents and its application in emergency planning: A case study, Saf Sci. 106 (2018) 203–218. https://doi.org/10.1016/j.ssci.2018.03.021.
[13] S.S. Tripathy, U. Bhatia, M. Mohanty, S. Karmakar, S. Ghosh, Flood evacua tion during pandemic: a multi-objective framework to handle compound hazard, Environ Res Lett. 16 (2021) 034034. https://doi.org/10.1088/1748-9326/abda70.
[14] L. Na, S. Xueyan, Q. Mingliang, A Bi-objective Evacuation Routing Engine ering Model with Secondary Evacuation Expected Costs, Systems Engineering Pr ocedia. 5 (2012) 1–7. https://doi.org/10.1016/j.sepro.2012.04.001.
[15] N. Insani, D. Akman, S. Taheri, J. Hearne, Short-notice flood evacuation pla n under dynamic demand in high populated areas, Int J Disaster Risk Reduct. 74 (2022) 102844. https://doi.org/10.1016/j.ijdrr.2022.102844.
[16] J. Zhao, M. Mao, B. Xie, A nuclear emergency partition evacuation framew ork based on comprehensive risk assessment, Int J Disaster Risk Reduct. 86 (202 3) 103543. https://doi.org/10.1016/j.ijdrr.2023.103543.
[17] X. Jia, G. Morel, H. Martell-Flore, F. Hissel, J.-L. Batoz, Fuzzy logic based decision support for mass evacuations of cities prone to coastal or river floods, Environ Modell Softw. 85 (2016) 1–10. https://doi.org/10.1016/j.envsoft.2016.07.018.
[18] D.K. Bird, G. Gísladóttir, Responding to volcanic eruptions in Iceland: from

the small to the catastrophic, Palgrave Communications. 4 (2018) 1–13. https://doi.org/10.1057/s41599-018-0205-6.

[19] L.-A. Gomez-Cunya, J. Tilt, D. Tullos, M. Babbar-Sebens, Perceived risk and preferences of response and recovery actions of individuals living in a floodplain community, Int J Disaster Risk Reduct. 67 (2022) 102645. https://doi.org/10.1016/j.ijdrr.2021.102645.

[20] T. Reichhardt, E. Check, E. Marris, After the flood, Nature. 437 (2005) 174–176. https://doi.org/10.1038/437174a.

[21] J. Bohannon, Directing the Herd: Crowds and the Science of Evacuation, Science. 310 (2005) 219–221. https://doi.org/10.1126/science.310.5746.219.

[22] M.K. Lindell, C.S. Prater, D.H. House, Cascadia Subduction Zone Residents' Tsunami Evacuation Expectations, Geosciences. 12 (2022) 189. https://doi.org/10.3390/geosciences12050189.

[23] Q. Xiong, Q. Zhu, Z. Du, X. Zhu, Y. Zhang, L. Niu, Y. Li, Y. Zhou, A Dynamic Indoor Field Model for Emergency Evacuation Simulation, ISPRS International Journal of Geo-Information. 6 (2017) 104. https://doi.org/10.3390/ijgi6040104.

[24] H.-M. Lyu, S.-L. Shen, A. Zhou, J. Yang, Perspectives for flood risk assessment and management for mega-city metro system, Tunnelling Underground Space Technol. 84 (2019) 31–44. https://doi.org/10.1016/j.tust.2018.10.019.

[25] G. Li, X. Wu, J.-C. Han, B. Li, Y. Huang, Y. Wang, Flood risk assessment by using an interpretative structural modeling based Bayesian network approach (ISM-BN): An urban-level analysis of Shenzhen, China, J Environ Manage. 329 (2023) 117040. https://doi.org/10.1016/j.jenvman.2022.117040.

[26] M. Zeleňáková, R. Fijko, S. Labant, E. Weiss, G. Markovič, R. Weiss, Flood risk modelling of the Slatvinec stream in Kružlov village, Slovakia, J Cleaner Prod. 212 (2019) 109–118. https://doi.org/10.1016/j.jclepro.2018.12.008.

[27] K. Zhang, M.H. Shalehy, G.T. Ezaz, A. Chakraborty, K.M. Mohib, L. Liu, An integrated flood risk assessment approach based on coupled hydrological-hydraulic modeling and bottom-up hazard vulnerability analysis, Environ Modell Softw. 148 (2022) 105279. https://doi.org/10.1016/j.envsoft.2021.105279.

[28] J. Nott, Extreme Events: A Physical Reconstruction and Risk Assessment, Cambridge University Press, 2006.

[29] X. Chen, M.-P. Kwan, Q. Li, J. Chen, A model for evacuation risk assessment with consideration of pre- and post-disaster factors, Comput Environ Urban. 36 (2012) 207–217. https://doi.org/10.1016/j.compenvurbsys.2011.11.002.

[30] S. Cai, J. Fan, W. Yang, Flooding Risk Assessment and Analysis Based on GIS and the TFN-AHP Method: A Case Study of Chongqing, China, Atmosphere. 12 (2021) 623. https://doi.org/10.3390/atmos12050623.

[31] A.R. Black, J.C. Burns, Re-assessing the flood risk in Scotland, Science of The Total Environment. 294 (2002) 169–184. https://doi.org/10.1016/S0048-9697(0

2)00062-1.

[32] Z. Wang, C. Lai, X. Chen, B. Yang, S. Zhao, X. Bai, Flood hazard risk assessment model based on random forest, J Hydrol. 527 (2015) 1130–1141. https://doi.org/10.1016/j.jhydrol.2015.06.008.

[33] H. Voogd, Multicriteria Evaluation with Mixed Qualitative and Quantitative Data, Environment and Planning B: Planning and Design. 9 (1982) 221–236. https://doi.org/10.1068/b090221.

[34] R.E. Steuer, P. Na, Multiple criteria decision making combined with finance: A categorized bibliographic study, Eur J Oper Res. 150 (2003) 496–515. https://doi.org/10.1016/S0377-2217(02)00774-9.

[35] J. Peng, J. Zhang, Urban flooding risk assessment based on GIS- game theory combination weight: A case study of Zhengzhou City, Int J Disaster Risk Reduct. 77 (2022) 103080. https://doi.org/10.1016/j.ijdrr.2022.103080.

[36] T. Lin, X. Liu, J. Song, G. Zhang, Y. Jia, Z. Tu, Z. Zheng, C. Liu, Urban waterlogging risk assessment based on internet open data: A case study in China, Habitat Int. 71 (2018) 88–96. https://doi.org/10.1016/j.habitatint.2017.11.013.

[37] M. Mejía-Navarro, E.E. Wohl, S.D. Oaks, Geological hazards, vulnerability, and risk assessment using GIS: model for Glenwood Springs, Colorado, in: M. Morisawa (Ed.), Geomorphology and Natural Hazards, Elsevier, Amsterdam, 1994: pp. 331–354. https://doi.org/10.1016/B978-0-444-82012-9.50025-6.

[38] X. Wang, H. Xie, A Review on Applications of Remote Sensing and Geographic Information Systems (GIS) in Water Resources and Flood Risk Management, Water. 10 (2018) 608. https://doi.org/10.3390/w10050608.

[39] P.D. Bates, A.P.J. De Roo, A simple raster-based model for flood inundation simulation, J Hydrol. 236 (2000) 54–77. https://doi.org/10.1016/S0022-1694(00)00278-X.

[40] M.S. Horritt, P.D. Bates, Evaluation of 1D and 2D numerical models for predicting river flood inundation, J Hydrol. 268 (2002) 87–99. https://doi.org/10.1016/S0022-1694(02)00121-X.

[41] C. Prudhomme, R.L. Wilby, S. Crooks, A.L. Kay, N.S. Reynard, Scenario-neutral approach to climate change impact studies: Application to flood risk, J Hydrol. 390 (2010) 198–209. https://doi.org/10.1016/j.jhydrol.2010.06.043.

[42] P. Blaikie, T. Cannon, I. Davis, B. Wisner, At Risk: Natural hazards, people's vulnerability and disasters, 2nd ed., Routledge, London, 2014. https://doi.org/10.4324/9780203714775.

[43] R.L. Church, T.J. Cova, Mapping evacuation risk on transportation networks using a spatial optimization model, Transportation Research Part C: Emerging Technologies. 8 (2000) 321–336. https://doi.org/10.1016/S0968-090X(00)00019-X.

[44] T.J. COVA, R.L. CHURCH, Modelling community evacuation vulnerability using GIS, Int J Geogr Inf Sci. 11 (1997) 763–784. https://doi.org/10.1080/136588197242077.

[45] H. Nasiri, M.J. Mohd Yusof, T.A. Mohammad Ali, An overview to flood vulnerability assessment methods, Sustainable Water Resources Management. 2 (2016) 331–336. https://doi.org/10.1007/s40899-016-0051-x.
[46] Proceedings of the Seminars on Flood Vulnerability Analysis and on the Principles of Floodplain Management for Flood Loss Prevention., in: UN, 1984. https://digitallibrary.un.org/record/69917 (accessed October 3, 2022).
[47] A. Darvishan, G.J. Lim, Dynamic network flow optimization for real-time evacuation reroute planning under multiple road disruptions, Reliab Eng Syst Saf. 214 (2021) 107644. https://doi.org/10.1016/j.ress.2021.107644.
[48] R.W. Perry, M.K. Lindell, Preparedness for Emergency Response: Guidelines for the Emergency Planning Process, Disasters. 27 (2003) 336–350. https://doi.org/10.1111/j.0361-3666.2003.00237.x.
[49] Y.-T. Hsu, S. Peeta, Risk-based spatial zone determination problem for stage-based evacuation operations, Transport Res C-Emer. 41 (2014) 73–89. https://doi.org/10.1016/j.trc.2014.01.013.
[50] T. Urbanik, Evacuation time estimates for nuclear power plants, J Hazard Mater. 75 (2000) 165–180. https://doi.org/10.1016/S0304-3894(00)00178-3.
[51] T.J. Cova, J.P. Johnson, Microsimulation of neighborhood evacuations in the urban-wildland interface, Environ Planning A. 34 (2002) 2211–2229. https://doi.org/10.1068/a34251.
[52] Y.-T. Hsu, S. Peeta, An aggregate approach to model evacuee behavior for no-notice evacuation operations, Transportation. 40 (2013) 671–696. https://doi.org/10.1007/s11116-012-9440-7.
[53] Hsu Y.-T., Peeta S., Clearance Time Estimation for Incorporating Evacuation Risk in Routing Strategies for Evacuation Operations, Netw Spat Econ. 15 (2015) 743–764.
[54] J. Duanmu, K.M. Taaffe, M. Chowdhury, R.M. Robinson, Simulation analysis for evacuation under congested traffic scenarios: a case study, SIMULATION. 88 (2012) 1379–1389. https://doi.org/10.1177/0037549712454688.
[55] F. Imamura, A. Muhari, E. Mas, M. Pradono, S. Wegscheider, J. Post, M. Sugimoto, Tsunami Disaster Mitigation by Integrating Comprehensive Countermeasures in Padang City, Indonesia, Journal of Disaster Research. 7 (2011). https://doi.org/10.20965/jdr.2012.p0048.
[56] M.A. Dulebenets, J. Pasha, O.F. Abioye, M. Kavoosi, E.E. Ozguven, R. Moses, W.R. Boot, T. Sando, Exact and heuristic solution algorithms for efficient emergency evacuation in areas with vulnerable populations, Int J Disaster Risk Reduct. 39 (2019) 101114. https://doi.org/10.1016/j.ijdrr.2019.101114.
[57] J.H. Lambert, A.I. Parlak, Q. Zhou, J.S. Miller, M.D. Fontaine, T.M. Guterbock, J.L. Clements, S.A. Thekdi, Understanding and managing disaster evacuation on a transportation network, Accid Anal Prev. 50 (2013) 645–658. https://doi.org/10.1016/j.aap.2012.06.015.

[58] J. Chen, J. Yu, J. Wen, C. Zhang, Z. Yin, J. Wu, S. Yao, Pre-evacuation Time Estimation Based Emergency Evacuation Simulation in Urban Residential Communities, Int J Environ Res Public Health. 16 (2019) 4599. https://doi.org/10.3390/ijerph16234599.
[59] W. Song, Y. Zhou, Road Travel Time Prediction Method Based on Random Forest Model, in: Y.-D. Zhang, J.K. Mandal, C. So-In, N.V. Thakur (Eds.), Smart Trends in Computing and Communications, Springer, Singapore, 2020: pp. 155–163. https://doi.org/10.1007/978-981-15-0077-0_17.
[60] Y. Zhang, A. Haghani, A gradient boosting method to improve travel time prediction, Transportation Research Part C: Emerging Technologies. 58 (2015) 308–324. https://doi.org/10.1016/j.trc.2015.02.019.
[61] E. Urbina, B. Wolshon, National review of hurricane evacuation plans and policies: a comparison and contrast of state practices, Transportation Research Part A: Policy and Practice. 37 (2003) 257–275. https://doi.org/10.1016/S0965-8564(02)00015-0.
[62] J. Qiu, L. Du, D. Zhang, S. Su, Z. Tian, Nei-TTE: Intelligent Traffic Time Estimation Based on Fine-Grained Time Derivation of Road Segments for Smart City, IEEE Trans Ind Informat. 16 (2020) 2659–2666. https://doi.org/10.1109/TII.2019.2943906.
[63] M.G.R. Fahad, R. Nazari, P. Bhavsar, M. Jalayer, M. Karimi, A decision-support framework for emergency evacuation planning during extreme storm events, Transportation Research Part D: Transport and Environment. 77 (2019) 589–605. https://doi.org/10.1016/j.trd.2019.09.024.
[64] M. Borowska-Stefańska, L. Balážovičová, K. Goniewicz, M. Kowalski, P. Kurzyk, M. Masný, S. Wiśniewski, M. Žoncová, A. Khorram-Manesh, Emergency management of self-evacuation from flood hazard areas in Poland, Transportation Research Part D: Transport and Environment. 107 (2022) 103307. https://doi.org/10.1016/j.trd.2022.103307.
[65] M. Borowska-Stefańska, M. Kowalski, S. Wiśniewski, M.A. Dulebenets, The impact of self-evacuation from flood hazard areas on the equilibrium of the road transport, Saf Sci. 157 (2023) 105934. https://doi.org/10.1016/j.ssci.2022.105934.
[66] K. Kohei, I. Daichi, S. Takumi, Y. Yuko, T. Hisatoshi, M. Yasuhiro, Study on Decision Making Support of Evacuation Guidance with a Novel Estimation of Evacuation Time considering Lead Time of Disaster Strike, Proceeding of the Institute of Social Safety Science. 39 (2021) 401–409.
[67] L. Breiman, Random Forests, Mach Learn. 45 (2001) 5–32. https://doi.org/10.1023/A:1010933404324.
[68] Y. Liu, H. Wu, Prediction of Road Traffic Congestion Based on Random Forest, in: 2017 10th International Symposium on Computational Intelligence and Design (ISCID), 2017: pp. 361–364. https://doi.org/10.1109/ISCID.2017.216.
[69] B. Yu, H. Wang, W. Shan, B. Yao, Prediction of Bus Travel Time Using R

andom Forests Based on Near Neighbors, Comput-Aided Civ Infrastruct Eng. 33 (2018) 333–350. https://doi.org/10.1111/mice.12315.

[70] L. Breiman, Bagging predictors, Mach Learn. 24 (1996) 123–140. https://doi.org/10.1007/BF00058655.

[71] T.K. Ho, The random subspace method for constructing decision forests, IEEE Trans Pattern Anal Mach Intell. 20 (1998) 832–844. https://doi.org/10.1109/34.709601.

[72] Y. Amit, D. Geman, Shape Quantization and Recognition with Randomized Trees, Neural Comput. 9 (1997) 1545–1588. https://doi.org/10.1162/neco.1997.9.7.1545.

[73] T.K. Ho, Random decision forests, in: Proceedings of 3rd International Conference on Document Analysis and Recognition, 1995: pp. 278–282 vol.1. https://doi.org/10.1109/ICDAR.1995.598994.

[74] B. Qiu, W. (David) Fan, Machine Learning Based Short-Term Travel Time Prediction: Numerical Results and Comparative Analyses, Sustainability. 13 (2021) 7454. https://doi.org/10.3390/su13137454.

[75] J.H. Friedman, J.J. Meulman, Multiple additive regression trees with application in epidemiology, Stat Med. 22 (2003) 1365–1381. https://doi.org/10.1002/sim.1501.

[76] J. Cheng, G. Li, X. Chen, Research on Travel Time Prediction Model of Freeway Based on Gradient Boosting Decision Tree, IEEE Access. 7 (2019) 7466–7480. https://doi.org/10.1109/ACCESS.2018.2886549.

[77] R. b. Sharmila, N.R. Velaga, A. Kumar, SVM-based hybrid approach for corridor-level travel-time estimation, IET Intel Transport Syst. 13 (2019) 1429–1439. https://doi.org/10.1049/iet-its.2018.5069.

[78] D. Bauer, M. Tulic, Travel time predictions: should one model speeds or travel times?, European Transport Research Review. 10 (2018) 46. https://doi.org/10.1186/s12544-018-0315-7.

[79] A. Narayanan, N. Mitrovic, M.T. Asif, J. Dauwels, P. Jaillet, Travel Time Estimation Using Speed Predictions, in: 2015 IEEE 18th International Conference on Intelligent Transportation Systems, 2015: pp. 2256–2261. https://doi.org/10.1109/ITSC.2015.364.

[80] J.S. Armstrong, F. Collopy, Error measures for generalizing about forecasting methods: Empirical comparisons, Int J Forecasting. 8 (1992) 69–80. https://doi.org/10.1016/0169-2070(92)90008-W.

[81] Y. Han, H. Liu, P. Moore, Extended route choice model based on available evacuation route set and its application in crowd evacuation simulation, Simul Model Pract Theory. 75 (2017) 1–16. https://doi.org/10.1016/j.simpat.2017.03.010.

[82] Y. Deng, Y. Chen, Y. Zhang, S. Mahadevan, Fuzzy Dijkstra algorithm for shortest path problem under uncertain environment, Appl Soft Comput. 12 (2012) 1231–1237. https://doi.org/10.1016/j.asoc.2011.11.011.

[83] E.W. Dijkstra, others, A note on two problems in connexion with graphs, Numerische Mathematik. 1 (1959) 269–271.

[84] F. Mirahadi, B.Y. McCabe, EvacuSafe: A real-time model for building evacuation based on Dijkstra's algorithm, Journal of Building Engineering. 34 (2021) 101687. https://doi.org/10.1016/j.jobe.2020.101687.

[85] H. Wang, W. Mao, L. Eriksson, A Three-Dimensional Dijkstra's algorithm for multi-objective ship voyage optimization, Ocean Eng. 186 (2019) 106131. https://doi.org/10.1016/j.oceaneng.2019.106131.

[86] Y. Zhu, H. Li, Z. Wang, Q. Li, Z. Dou, W. Xie, Z. Zhang, R. Wang, W. Nie, Optimal Evacuation Route Planning of Urban Personnel at Different Risk Levels of Flood Disasters Based on the Improved 3D Dijkstra's Algorithm, Sustainability. 14 (2022) 10250. https://doi.org/10.3390/su141610250.

[87] G.G. Løvs, Models of wayfinding in emergency evacuations, Eur J Oper Res. 105 (1998) 371–389. https://doi.org/10.1016/S0377-2217(97)00084-2.

[88] W. Li, Y. Li, P. Yu, J. Gong, S. Shen, The Trace Model: A model for simulation of the tracing process during evacuations in complex route environments, Simul Model Pract Theory. 60 (2016) 108–121. https://doi.org/10.1016/j.simpat.2015.09.011.

[89] K. Yamamoto, X. Li, Safety Evaluation of Evacuation Routes in Central Tokyo Assuming a Large-Scale Evacuation in Case of Earthquake Disasters, Journal of Risk and Financial Management. 10 (2017) 14. https://doi.org/10.3390/jrfm10030014.

[90] S. Çolak, A. Lima, M.C. González, Understanding congested travel in urban areas, Nat Commun. 7 (2016) 10793. https://doi.org/10.1038/ncomms10793.

[91] Traffic Capacity of Roads, Japan Road Association, 1984.

[92] T.J. Cova, J.P. Johnson, A network flow model for lane-based evacuation routing, Transportation Research Part A: Policy and Practice. 37 (2003) 579–604. https://doi.org/10.1016/S0965-8564(03)00007-7.

[93] H. Spiess, Technical Note—Conical Volume-Delay Functions, Transport Sci. 24 (1990) 153–158. https://doi.org/10.1287/trsc.24.2.153.

[94] US Bureau of Public Roads Office of Planning Urban Planning, Traffic assignment manual for application with a large, high speed computer, US Department of Commerce, 1964.

[95] K. Feng, N. Lin, Reconstructing and analyzing the traffic flow during evacuation in Hurricane Irma (2017), Transportation Research Part D: Transport and Environment. 94 (2021) 102788. https://doi.org/10.1016/j.trd.2021.102788.

[96] National Research Council (U.S.), ed., Highway capacity manual, Transportation Research Board, National Research Council, Washington, D.C, 2000.

[97] F. Yamada, R. Kakimoto, M. Yamamoto, T. Fujimi, N. Tanaka, Implementation of community flood risk communication in Kumamoto, Japan, J Adv Transport. 45 (2011) 117–128. https://doi.org/10.1002/atr.119.

[98] D. Yu, J. Yin, R.L. Wilby, S.N. Lane, J.C.J.H. Aerts, N. Lin, M. Liu, H. Yuan, J. Chen, C. Prudhomme, M. Guan, A. Baruch, C.W.D. Johnson, X. Tang, L. Yu, S. Xu, Disruption of emergency response to vulnerable populations during floods, Nature Sustainability. 3 (2020) 728–736. https://doi.org/10.1038/s41893-020-0516-7.

[99] Y.-H. Lee, Y.-C. Kim, H. Lee, Framework for selection of temporary disaster waste management sites for post-flood recovery in Seoul, South Korea, Int J Disaster Risk Reduct. 71 (2022) 102832. https://doi.org/10.1016/j.ijdrr.2022.102832.

[100] C. Dias, N.A. Rahman, A. Zaiter, Evacuation under flooded conditions: Experimental investigation of the influence of water depth on walking behaviors, Int J Disaster Risk Reduct. 58 (2021) 102192. https://doi.org/10.1016/j.ijdrr.2021.102192.

[101] G. Bernardini, E. Quagliarini, M. D’Orazio, M. Brocchini, Towards the simulation of flood evacuation in urban scenarios: Experiments to estimate human motion speed in floodwaters, Saf Sci. 123 (2020) 104563. https://doi.org/10.1016/j.ssci.2019.104563.

[102] E. Bosina, U. Weidmann, Estimating pedestrian speed using aggregated literature data, Physica A. 468 (2017) 1–29. https://doi.org/10.1016/j.physa.2016.09.044.

[103] K. Toda, Urban Flooding and Measures, Journal of Disaster Research. 2 (2007) 143–152. https://doi.org/10.20965/jdr.2007.p0143.

[104] Y. Zheng, X.-G. Li, B. Jia, R. Jiang, Simulation of pedestrians’ evacuation dynamics with underground flood spreading based on cellular automaton, Simul Model Pract Theory. 94 (2019) 149–161. https://doi.org/10.1016/j.simpat.2019.03.001.

[105] Dan Matsumoto, Y. Sawai, M. Yamada, Y. Namegaya, T. Shinozaki, D. Takeda, S. Fujino, K. Tanigawa, A. Nakamura, J.E. Pilarczyk, Erosion and sedimentation during the September 2015 flooding of the Kinu River, central Japan, Sci Rep. 6 (2016) 34168. https://doi.org/10.1038/srep34168.

[106] M. Ohki, T. Tadono, T. Itoh, K. Ishii, T. Yamanokuchi, M. Watanabe, M. Shimada, Flood Area Detection Using PALSAR-2 Amplitude and Coherence Data: The Case of the 2015 Heavy Rainfall in Japan, IEEE J Sel Topics Appl Earth Observ Remote Sens. 12 (2019) 2288–2298. https://doi.org/10.1109/JSTARS.2019.2911596.

[107] Levee Collapse of the Kinu River: How Did Joso City Residents Evacuate?, (n.d.). https://www.nhk.or.jp/bunken/english/research/domestic/20160801_6.html (accessed June 9, 2022).

[108] RRI model - ICHARM The International Centre for Water Hazard, (n.d.). https://www.pwri.go.jp/icharm/research/rri/index.html (accessed January 13, 2023).

[109] Location of evacuation shelters/ Joso City Homepage, (n.d.). http://www.city.joso.lg.jp/jumin/anzen/bosai/1419259176253.html (accessed September 26, 2022).

[110] Micro Geodata Forum, (n.d.). http://microgeodata.jp/index.html (accessed January 23, 2023).

[111]About GSI | GSI HOME PAGE, (n.d.). https://www.gsi.go.jp/ENGLISH/page_e30003.html (accessed September 8, 2022).

[112] V. Rözer, A. Peche, S. Berkhahn, Y. Feng, L. Fuchs, T. Graf, U. Haberlandt, H. Kreibich, R. Sämann, M. Sester, B. Shehu, J. Wahl, I. Neuweiler, Impact-Based Forecasting for Pluvial Floods, Earth's Future. 9 (2021) 2020EF001851. https://doi.org/10.1029/2020EF001851.

[113] Y. Sawada, K. Okamoto, M. Kunii, T. Miyoshi, Assimilating Every-10-minute Himawari-8 Infrared Radiances to Improve Convective Predictability, Journal of Geophysical Research: Atmospheres. 124 (2019) 2546–2561. https://doi.org/10.1029/2018JD029643.

[114] K. Takahashi, Y. Kajitani, H. Saito, M. Kuroki, A proposal for mutual-aid-type distributed evacuation based on residents' evacuation intentions in a hilly and mountainous area of Japan, Int J Disaster Risk Reduct. 82 (2022) 103366. https://doi.org/10.1016/j.ijdrr.2022.103366.

[115] Y. Alabbad, J. Mount, A.M. Campbell, I. Demir, Assessment of transportation system disruption and accessibility to critical amenities during flooding: Iowa case study, Science of The Total Environment. 793 (2021) 148476. https://doi.org/10.1016/j.scitotenv.2021.148476.